Numerical Analysis and Experimental Evaluation for Low-Temperature and Dense Plasma Generation using Pulsed Power Discharge Device

Takashi Kikuchi, Hirotaka Saito, Ryota Hayashi, Toru Sasaki, Nob. Harada

Department of Electrical Engineering, Nagaoka University of Technology

ABSTRACT

Using both numerical and experimental approaches are applied to evaluation for low-temperature and dense plasma. To investigate properties of low-temperature and dense plasma, the numerical simulation of time-dependent one-dimensional thermal diffusion with radiative transfer is carried out in a compact pulsed power discharge device. The simulation result is useful to understand the thermodynamic phenomena during the discharge in comparison with the experimental result.

Keywords

Numerical Simulation, Pulsed Power Discharge, Warm Dense Matter, Low-Temperature Dense Plasma, Thermal Diffusion, Radiative Transport, Opacity, Absorption Coefficient

1 Introduction

Property data of low-temperature and dense plasma and warm dense matter (WDM) are important to control implosion dynamics in a fuel pellet of inertial confinement fusion (ICF) [1]. Because the material phase of the fuel pellet changes from a solid to plasma due to irradiation of energy drivers, such as intense lasers, high power X-ray, and high-current heavy ion beams.

However, the condition is in an extreme high pressure situation. For this reason, it is difficult to create statically the condition with measurable setup. As a result, the properties in WDM and low-temperature dense plasma are unclear.

Pulsed power discharge devices were used to generate the extreme state of matter [2–4]. For the generation of WDM with a well-defined condition, the apparatus with isochoric heating using sapphire hollow capillary as a rigid body wall was proposed by using a table-top pulsed power supply [5,6]. In the experimental apparatus, the emission from the heated sample was observable due to the transparent sapphire capillary.

In our previous study, we numerically investigate to generate the low-temperature and dense plasma by using pulsed power discharge devices to obtain the properties of low-temperature and dense plasmas [7]. In this study, we calculate simultaneously the condition with radiative transport to obtain the properties of low-temperature and dense plasmas.

2 Simulation Model

In the experimental setup, the fluid dynamics of the sample plasma is limited by the capillary [5,6]. For this reason, we can calculate the phenomena in the foam/plasma ignoring the hydrodynamics. In this study, we solve simultaneously the thermal diffusion and radiative transfer, numerically.

2.1 Computational Box

The computational box is shown in Fig. 1. In this apparatus, a foamed copper is used as a sample, and is surrounded with a hollow sapphire capillary.

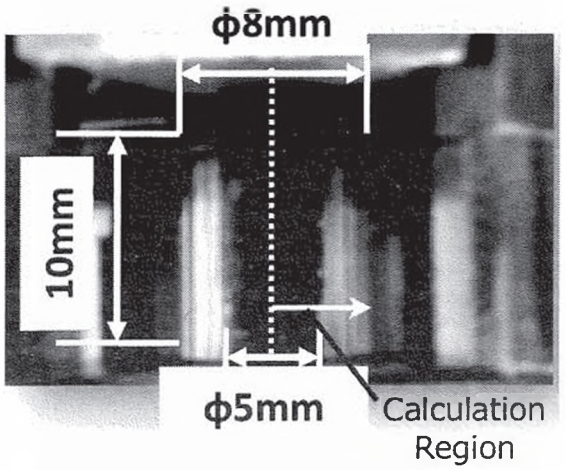

Figure 1: Computational box for time-dependent one-dimensional thermal diffusion and radiative transfer equations with cylindrical symmetry configuration. The inner region ($0 < r < 2.5$ mm) is the foamed copper as a sample, and the outer region (2.5 mm $< r <$ 4 mm) is the sapphire as a rigid capillary.

Time-dependent one-dimensional thermal diffusion equation with cylindrical symmetry configuration is numerically solved to simulate the low-temperature and dense plasma generation in the compact pulsed power discharge experiment [5,6].

The density of the foamed copper surrounded in the hollow capillary is 0.1 times the solid density (8920 kg/m^3). The mass density of the sapphire is 3970 kg/m^3 as the solid. In this setup, the fluid dynamics of the sample plasma is limited by the capillary. For this reason, we only calculate the thermodynamics in the foam/plasma without the fluid dynamics of plasma.

Since the sample is a foamed material, we assumed that the skin effect can be ignored. As a result, the discharge current distribution is assumed as uniform in the copper region.

2.2 Thermal Diffusion

The temperature T of the sample is the function of spacial position and time t, and the thermodynamics is given by

$$\rho C_v \frac{\partial T}{\partial t} = \nabla \cdot (\kappa \nabla T) + S_J - S_r, \qquad (1)$$

where ρ is the mass density of the sample, C_v is the specific heat, κ is the thermal conductivity, S_J is the source term due to Joule heating, and S_r is the source term due to the absorption and emission of radiation, respectively. The source term due to Joule heating is obtained by

$$S_J = \frac{P_{in}}{V_{foam}}, \qquad (2)$$

where P_{in} is the input power from the pulse power supply and V_{foam} is the volume of the sample.

The above equation is rewritten by

$$\rho C_v \frac{\partial T}{\partial t} = \frac{1}{r}\frac{\partial}{\partial r}\left(r\kappa \frac{\partial T}{\partial r}\right) + S_J - S_r, \qquad (3)$$

along the radius r in the cylindrical coordinate.

2.3 Thermodynamic Property

The initial temperature is set as 300 K by a room temperature in the whole computational region. The conventional thermal property data of copper in solid, liquid, and gas phases are given by Refs. [8–11]. Figures 2 and 3 show the summary of the thermal conductivity and the specific heat as a function of temperature.

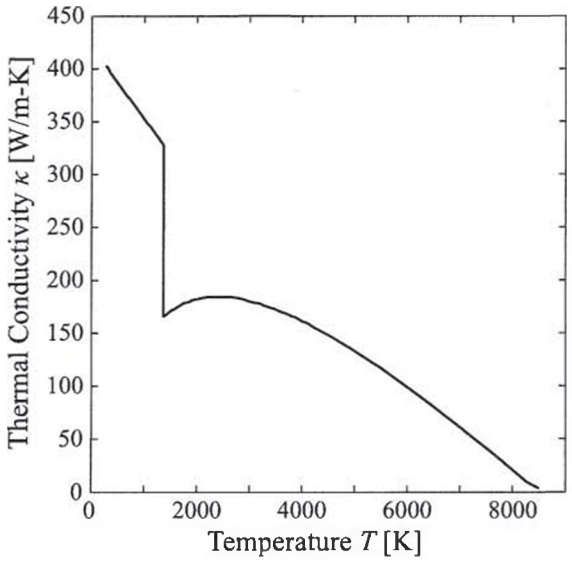

Figure 2: Thermal conductivity as a function of temperature for copper [8,9].

In the sapphire region, the material parameters for numerical simulation are 42 W/m-K for the thermal conductivity and 750 J/kg-K for the specific heat, as room temperature values.

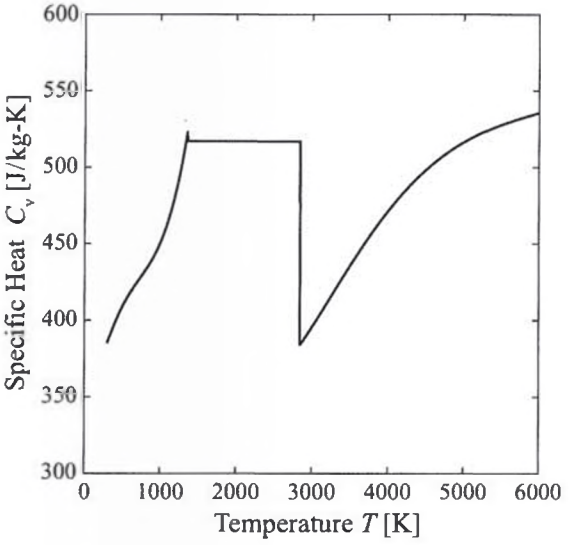

Figure 3: Specific heat as a function of temperature for copper [10, 11].

2.4 Radiative Transfer

The radiative transfer equation is solved by the diffusion approximation. The diffusion equation for the radiation energy density E_ν at the frequency ν is [12]

$$\frac{\partial E_\nu}{\partial t} - \nabla \cdot \left(\frac{c}{3\,\kappa_\nu} \nabla E_\nu \right) = 4\pi\,\eta_\nu - \kappa_\nu c E_\nu, \quad (4)$$

where c is the speed of light, κ_ν and η_ν are the opacity and the emissivity at the frequency ν, respectively. In the assumption as local thermal equilibrium (LTE),

$$\eta_\nu = B_\nu\,\kappa_\nu, \quad (5)$$

where B_ν is the distribution function of photon in a frequency ν. As a result, the radiation diffusion equation can be rewritten by

$$\frac{\partial E_\nu}{\partial t} - \nabla \cdot \left(\frac{c}{3\,\kappa_\nu} \nabla E_\nu \right) = (4\pi B_\nu - c\,E_\nu)\,\kappa_\nu. \quad (6)$$

For one-dimensional case, the above equation is rewritten by

$$\frac{\partial E^g}{\partial t} - \frac{1}{r}\frac{\partial}{\partial r}\left(r \frac{c}{3\,\kappa_{\rm R}^g} \frac{\partial E^g}{\partial r} \right) = (4\pi\,B^g - c\,E^g)\,\kappa_{\rm P}^g, \quad (7)$$

along the radius r in the cylindrical coordinate with a multi-group approximation in the frequency domain [13]. Here index g indicates the group number, and

$$\frac{1}{{\kappa_{\rm R}}^g} = \frac{\int_{\nu_g}^{\nu_{g+1}} 1/\kappa_\nu\,\partial B_\nu/\partial k_{\rm B}T\,d\nu}{\int_{\nu_g}^{\nu_{g+1}} \partial B_\nu/\partial k_{\rm B}T\,d\nu} \quad (8)$$

is the Rosseland absorption coefficient at g th group [14] in LTE approximation,

$${\kappa_{\rm P}}^g = \frac{\int_{\nu_g}^{\nu_{g+1}} \kappa_\nu\,B_\nu\,d\nu}{\int_{\nu_g}^{\nu_{g+1}} B_\nu\,d\nu} \quad (9)$$

is the Planck absorption coefficient at g th group [14], $k_{\rm B}$ is the Boltzmann constant. Here

$$E^g = \frac{\int_{\nu_g}^{\nu_{g+1}} E_\nu\,d\nu}{\int_{\nu_g}^{\nu_{g+1}} d\nu} \quad (10)$$

is the radiation energy density at g th group, and the blackbody intensity is

$$B^g = \frac{\int_{\nu_g}^{\nu_{g+1}} B_\nu\,d\nu}{\int_{\nu_g}^{\nu_{g+1}} d\nu}. \quad (11)$$

The source term due to the radiation, introduced in the thermal diffusion equation, is obtained by

$$S_{\rm r} = \sum_g (4\pi B^g - c\,E^g)\,\kappa_{\rm P}^g. \quad (12)$$

The radiative transfer in an optically thin region is expressed by the flux limited diffusion [15]

$$\mathbf{F}_\nu = -\frac{c\lambda}{\kappa_\nu}\nabla E_\nu, \quad (13)$$

where λ is the flux limiter [15]. For the optically thin limit, the flux limited diffusion is written by

$$|\mathbf{F}_\nu| = cE_\nu. \quad (14)$$

For this reason, the radiative transfer is calculated by approximately

$$\frac{\partial E^g}{\partial t} = -\frac{c}{r}\frac{\partial E^g}{\partial r}, \quad (15)$$

in the sapphire domain.

2.5 Opacity

In this study, we calculate the radiative transfer as one-group diffusion equation in the frequency domain.

The Planck mean opacity [cm^2/g] [16] can be calculated by

$$\chi_{\rm P} = \frac{\kappa_{\rm P}}{\rho} = 0.43\frac{Z^3}{A^2}\rho T^{-7/2}, \quad (16)$$

and the Rosseland mean opacity [cm^2/g] [16] is

$$\chi_R = \frac{\kappa_R}{\rho} = 0.014 \frac{Z^3}{A^2} \rho T^{-7/2}, \qquad (17)$$

where ρ is the (mass) density [g/cm^3], T is the temperature [keV], Z and A are the nuclear charge and mass number, respectively.

Figure 4 shows the opacities normalized by the mass density. The opacities are used to calculate

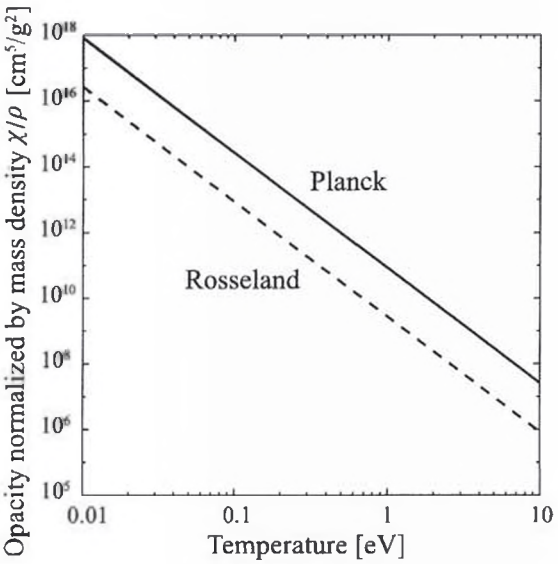

Figure 4: Planck (solid line) and Resseland (dashed line) mean opacities normalized by mass density as a function of temperature for copper calculated by Eqs. (16) and (17), respectively.

the radiation diffusion equation in the foamed copper region.

3 Calculation Result

Figure 5 shows the input power history, which is given by the corresponding experimental data [5, 6]. Figure 6 shows the temperature distribution as the numerical simulation result of time-dependent phenomena in the copper foam and the sapphire capillary regions. The numerical simulation confirmed that the sample is achieved to the temperature generating WDM. The result can be compared with the experimental result to understand the phenomena in the capillary during the discharge [5,6]. The result indicates that the temperature at the interface between the copper foam and the sapphire capillary is diffused, and the temperature around the edge of copper region is reduced due to the difference of the heat capacities.

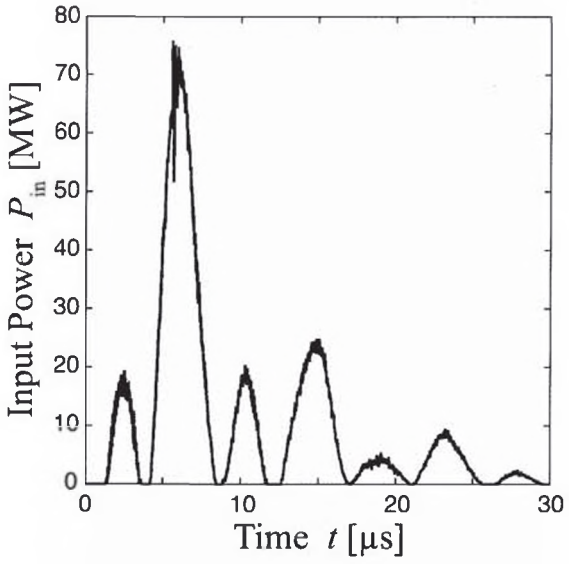

Figure 5: Input power history by pulsed power discharge experiment.

Figure 7 shows the radiation energy density solved numerically. The radiation energy density profile corresponds to the temperature distribution as shown in Fig. 6. Since the sample temperature is not high, the radiation energy density is low in comparison with the thermal energy of the sample. Figure 7 implies that the radiation energy density history can be observed by the thermal and radiative diffusion system. To improve the opacity model, the radiative transfer calculation can be confirmed with the experimental results. As a result, the calculation result can support the experimental results through the radiation distribution.

4 Conclusion

Using both the numerical and experimental approaches were carried out to evaluate the low temperature and dense plasma. In this study, the numerical simulation of time-dependent one-dimensional thermal diffusion with radiative transfer was carried out in the experimental results using the compact pulsed power discharge device. The simulation result was useful to understand the thermodynamic properties during the discharge in comparison with the experimental results. To improve the opacity model and multi-group approximation,

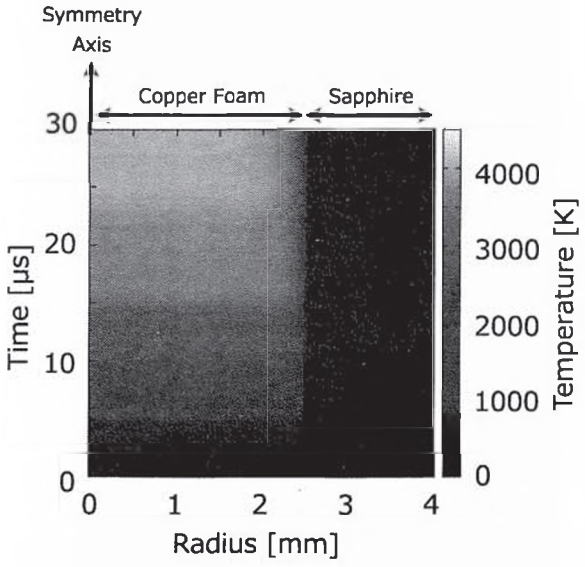

Figure 6: Temperature distribution in radial direction as a function of time.

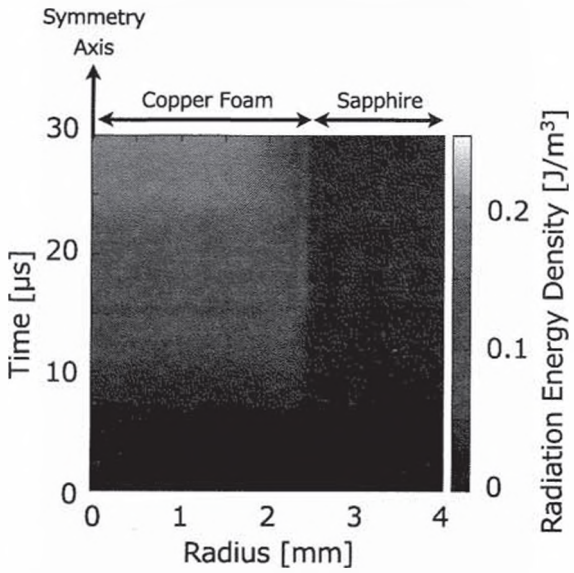

Figure 7: Radiation energy density in radial direction as a function of time.

the radiative transfer calculation will be confirmed with the experimental results in our near future work.

The compact pulsed power discharge device used is useful tool to generate the low-temperature and dense plasma condition. Although typical implosion time for ICF is in several-10 ns [17], the discharge time (several-10 μs) driven by the compact pulsed power device is not suitable to observe the ultrafast phenomenon during the implosion process. The nominal parameters of the intense pulsed power generator "ETIGO-II" [18] are 1 MV- 1 MA - 50 ns (FWHM) in the current condition. Using this intense pulsed power device, the volumetric dense plasma generation is expected, even in the short pulse duration. The numerical simulation with the experimental approach by using the above apparatus is also one of our future stages.

References

[1] S. ATZENI and J. MEYER-TER-VEHN, *The Physics of Inertial Fusion: Beam Plasma Interaction, Hydrodynamics, Hot Dense Matter* (Oxford Univ., N.Y., 2004).

[2] A.W. DESILVA and J.D. KATSOUROS, *Phys. Rev.* **E 57**, 5945 (1998).

[3] T. SASAKI, M. NAKAJIMA, T. KAWAMURA, and K. HORIOKA, *Phys. Plasmas*, **17**, 084501 (2010).

[4] T. SASAKI, T. SUZUKI, Y. AMANO, Y. MIKI, T. KIKUCHI, Nob. HARADA, and K. HORIOKA, *IOP Conf. Series: Material Science and Engineering*, **21**, 012016 (2011).

[5] Y. AMANO, Y. MIKI, T. SASAKI, T. KIKUCHI, and Nob. HARADA, *submitted to Rev. Sci. Instrum.*

[6] Y. MIKI, Y. AMANO, T. SASAKI, T. KIKUCHI, and Nob. HARADA, *in this proceedings.*

[7] T. KIKUCHI, T. SASAKI, Nob. HARADA, W. JIANG, and A. TOKUCHI, "Numerical Analysis for Low-Temperature and Dense Plasma Generation using Pulsed Power Discharge Devices", *Plasma 2011*, Kanazawa, Nov. 22-25, (2011) 23P162-R.

[8] C.Y. HO, R.W. POWELL, and P.E. LILEY, "Thermal Conductivity of the Elements", *JPCRD*, **1(2)**, pp.279-422 (1972).

[9] C.Y. HO, R.W. POWELL, and P.E. LILEY, "Thermal Conductivity of the Elements: A Comprehensive Review", *JPCRD*, **3(Suppl. 1)**, pp.1-796 (1974).

[10] NIST Standard Reference Database Number 69, http://webbook.nist.gov/chemistry/

[11] M.W. CHASE, NIST-JANAF Thermochemical Tables, Fourth Edition, *J. Phys. Chem. Ref. Data*, Monograph 9 (1998).

[12] J.I. CASTOR, *Radiation Hydrodynamics* (Cambridge University Press, 2007).

[13] S. ATZENI and J. MEYER-TER-VEHN, *The Physics of Inertial Fusion: Beam Plasma Interaction, Hydrodynamics, Hot Dense Matter* (Oxford Univ., N.Y., 2004) Chap. 7.3.

[14] L. DRSKA and M. SINOR, *Computer Phys. Communications*, **997**, pp.1-12 (1996).

[15] C.D. LEVERMORE and G.C. POMRANING, *Astrophysical Journal*, **248**, pp.321-334 (1981).

[16] S. ATZENI and J. MEYER-TER-VEHN, *The Physics of Inertial Fusion: Beam Plasma Interaction, Hydrodynamics, Hot Dense Matter* (Oxford Univ., N.Y., 2004) p.356.

[17] T. KIKUCHI, et al., *IEEJ Trans. FM*, **125**, pp.515-520 (2005).

[18] W. JIANG, T. SAKAGAMI, K. MASUGATA, and K. YATSUI, *Jpn. J. Appl. Phys.*, **32**, L752-L754 (1993).